Research Square

Preprints are preliminary reports that have not undergone peer review.
They should not be considered conclusive, used to inform clinical practice,
or referenced by the media as validated information.

# Facile synthesis of dual-emission carbon dots and fabrication of Poly(vinyl alcohol)/Alginate/carbon dots films for selective fluorescence detection and smartphone-assisted monitoring of $NO_2$- and $Fe^{3+}$ in water

**Nguyen Ba Hung**
Vietnam Military Medical University
**Duong Duy Son**
Vietnam Military Medical University
**Vu Tan Phat**
Vietnam Military Medical University
**Do Viet Anh**
Vietnam Military Medical University
**Tran Thi Bich Lan**
Vietnam Military Medical University
**Luu Thi Van**
Vietnam Military Medical University
**Ban Dieu Linh**
Vietnam Military Medical University
**Nguyen Trong Nghia**
Vietnam National University, Hanoi
**Nguyen Minh Hoang**
nguyenminhhoanghh1@gmail.com
Vietnam Military Medical University

**Research Article**

**Keywords:** carbon dots, Poly(vinyl alcohol)/Alginate, dual-emission, nitrite, ferric ions

**Posted Date:** April 14th, 2026

**DOI:** https://doi.org/10.21203/rs.3.rs-9287908/v1

**License:** This work is licensed under a Creative Commons Attribution 4.0 International License.
Read Full License

**Additional Declarations:** No competing interests reported.

---

**Version of Record:** A version of this preprint was published at Journal of Nanoparticle Research on June 25th, 2026. See the published version at https://doi.org/10.1007/s11051-026-06701-2.

# Abstract

Carbon dots (CDs) have demonstrated high selectivity as fluorescent probes for pollutant detection. However, most reported systems rely on single-emission intensity responses, which are susceptible to signal fluctuation, environmental interference, and limited reliability in complex matrices. In addition, translating solution-phase CD sensors into stable solid-state platforms remains challenging due to background fluorescence and the potential leaching of nanomaterials. Herein, dual-emission CDs with characteristic peaks at 420 and 520 nm were synthesized, enabling selective discrimination of and Fe3+ via distinct quenching responses. The sensor exhibited excellent linearity with low detection limits of 0.12 ppm for and 0.17 ppm for Fe3+. Crucially, a flexible PVA/Alg/CD fluorescent film was fabricated by immobilizing the CDs within a co-polymer PVA/alginate matrix. The composite film displayed strong and uniform blue fluorescence under 365 nm UV excitation, excellent optical stability, and effective confinement of CDs without observable leaching in aqueous environments. Upon exposure to $NO_2$-, the film exhibited rapid and visually distinguishable fluorescence quenching, with intensity decreasing progressively over the 0 - 50 ppm range. Notably, smartphone-assisted RGB image analysis enabled quantitative evaluation of fluorescence changes, generating linear calibration curves with coefficients of determination exceeding 0.93, consistent with spectroscopic measurements. These findings highlight the strong potential of the PVA/Alg/CDs film as a portable, solid-state platform for on-site water quality monitoring.


# 1. Introduction

The contamination of water resources by inorganic ions poses a persistent threat to environmental safety and human health. Among these pollutants, nitrite ($NO_2^-$) and ferric ions ($Fe^{3+}$) are of particular concern due to their widespread occurrence and adverse biological effects [1, 2]. Excessive nitrite exposure is closely associated with methemoglobinemia and the formation of carcinogenic N-nitrosamines [3], whereas abnormal $Fe^{3+}$ concentrations can disrupt aquatic ecosystems and induce oxidative stress [4]. Consequently, the development of selective, sensitive, and practical methods for monitoring$NO_2^-$ and $Fe^{3+}$ in aqueous environments is of critical importance [5, 6].

Fluorescence-based sensing has emerged as an attractive analytical strategy owing to its high sensitivity, rapid response, and operational simplicity [7, 8]. Carbon dots (CDs) have received considerable attention as fluorescent probes because of their strong photoluminescence, excellent water solubility, chemical stability, low toxicity, and abundant surface functional groups [9]. As a result, few CD-based sensors have been reported for the detection of various metal ions and anions, including $Fe^{3+}$ and $NO_2^-$ [10–12].

Despite these advances, most CD-based fluorescence sensors rely on single-emission intensity changes, predominantly fluorescence quenching, which inherently limits their discriminative capability [9, 13]. For example, Wang et al. [10] developed N, B-doped carbon dots for nitrite detection, achieving an ultralow detection limit of 6.6 nM with a wide linear range from 2 μM to 1 mM. However, the sensing output

depended solely on fluorescence attenuation at a single emission wavelength, making the response susceptible to interference from other quenching species in complex water matrices. Similarly, Cheng et al. [14] synthesized coal-derived carbon dots for $Fe^{3+}$ detection. The CDs can detect $Fe^{3+}$ via a turn-off fluorescence mechanism governed by the inner filter effect, with a detection limit of approximately 600 nM and a linear range of 2 to 100 μM. Nevertheless, the fluorescence quenching induced by $Fe^{3+}$ showed significant spectral overlap with other strongly absorbing or coordinating ions, such as $Cu^{2+}$ and $Pb^{2+}$, particularly at elevated concentrations, hindering unambiguous ion discrimination.

Beyond optical selectivity, practical water monitoring further requires solid-state sensing platforms with low background interference, high signal stability, and resistance to water-induced degradation [15–17]. Many existing solid-state CD sensors employ paper substrates [18–20], which exhibit strong intrinsic autofluorescence under UV excitation, resulting in high background signals and reduced sensitivity. Likewise, single-polymer matrices such as poly(vinyl alcohol) [21, 22] often provide insufficient confinement of CDs, leading to gradual leaching in aqueous environments and compromised sensing stability [23].

In this work, we report a dual-emission carbon-dot-based sensing system capable of unambiguously discriminating between $NO_2^-$ and $Fe^{3+}$ ions through two well-resolved fluorescence emission bands. The two emission channels respond selectively and independently: $Fe^{3+}$ preferentially quenches one emission band via coordination-induced electron transfer, whereas $NO_2^-$ selectively modulates the other through a distinct photophysical pathway. This dual-emission behavior enables reliable ion discrimination beyond conventional single-intensity sensing. Furthermore, the CDs are immobilized within a PVA–alginate copolymer film to realize practical solid-state sensing. The hydrophilic interpenetrating polymer network exhibits high water absorbance and excellent wettability, facilitating rapid ion diffusion and uniform interfacial contact, while simultaneously providing strong physical confinement of CDs to suppress aggregation and leaching. Owing to the high fluorescence intensity of the composite film, changes in $NO_2^-$ concentration can be directly visualized and quantitatively analyzed using smartphone-assisted imaging, highlighting its potential for portable and user-friendly water monitoring applications.

## 2. Experimental

# 2.1. Materials

All chemicals and solvents were of analytical grade and used as received without further purification. Glucose, citric acid, glycerol, and ethylenediaminetetraacetic acid were purchased from Merck and Xilong, respectively, and used to synthesize CDs. Poly(vinyl alcohol) and sodium alginate, employed for the fabrication of the PVA/Alg/CDs composite film, were obtained from Macklin. For heavy metal and nitrite detection experiments, standard solutions of $Fe(NO_3)_3$ (1000 $mgL^{-1}$) and $NaNO_2$ were purchased

from Merck. Other metal salts and inorganic compounds, including $Pb(NO_3)_2$, $Cu(NO_3)_2$, $FeCl_2.4H_2O$, NaCl, KCl, $MgCl_2.4H_2O$, $CaCl_2$, $Na_2SO_4$, and $Na_2CO_3$, were obtained from Xilong.

## 2.2. Characterizations

The morphology of the as-prepared carbon dots was characterized by high-resolution transmission electron microscopy (HR-TEM, JEOL JEM-2100). Surface functional groups were identified using an Affinity-1 S Fourier transform infrared spectrometer (Shimadzu, Kyoto, Japan). The UV-vis absorption spectra were recorded with a Hach DR6000 UV-Vis spectrophotometer, while photoluminescence measurements were carried out using a Fluorolog FL3 spectrometer (Jobin Yvon Spex) and a Cary Eclipse fluorescence spectrometer.

## 2.3. Synthesis of CDs

CDs were synthesized via a modified one-pot hydrothermal method based on our previously reported procedure [24]. In particular, glucose (0.1 g), citric acid (0.2 g), sodium fluorescein (0.05 g), and ethylenediaminetetraacetic acid (EDTA, 0.1 g) were dissolved in a mixed solvent consisting of 20 mL glycerol and 50 mL deionized water under continuous stirring to form a homogeneous precursor solution. The solution was transferred into a 100 mL Teflon-lined stainless-steel autoclave and subjected to hydrothermal treatment at 180°C for 12 h.

After completion of the reaction and natural cooling to room temperature, the resulting suspension was centrifuged at 10000 rpm to remove large particulates. The collected supernatant containing the CDs was purified by dialysis using a 3.5 kDa molecular weight cut-off membrane (Spectra/Por 3) against deionized water for 48 h, with the dialysis medium replaced every 12 h to ensure thorough removal of unreacted precursors and byproducts. The purified CD dispersion was collected and denoted as CDs.

To obtain solid CDs, the purified dispersion was frozen at -60°C for 48 h and subsequently lyophilized at -30°C under a vacuum of 0.01 bar for an additional 48 h. The resulting brown powder was stored at 4°C for further characterization and applications.

## 2.4. Fabrication of PVA/Alg/CDs film

The PVA/Alg/CDs film was prepared by incorporating CDs into a PVA-Alginate copolymer matrix. Briefly, 20 mL of PVA solution (1% w/v), 20 mL of sodium alginate solution (2% w/v), and 10 mL of CDs solution (5 mg $L^{-1}$) were vigorously mixed to obtain a homogeneous casting solution. The mixture was then poured into a silicone mold (10 × 10 cm). To induce ionic crosslinking and form a hydrogel film, 50 mL of $CaCl_2$ solution (0.04 M) was added to the mold and allowed to react until gelation was complete.

The resulting hydrogel film was removed, then dried at 40°C for 48 h to remove residual water and obtain a thin freestanding film. The dried film was labeled as PVA/Alg/CDs film and stored at 4°C for subsequent characterization and applications.

## 2.5. Detection of pollutant ions

For nitrite ($NO_2^-$) sensing, 1 mL of the as-prepared CD solution (5 $mgL^{-1}$) was mixed with 2 mL of $NO_2^-$ solutions at different concentrations ranging from 0 to 50 ppm. After incubation at room temperature for 10 min, the photoluminescence (PL) spectra of the mixtures were recorded at excitation wavelengths of 320 and 400 nm. The detection of $Fe^{3+}$ ions was performed under identical experimental conditions.

The limit of detection (LOD) was calculated according to the following equation:

$$LOD = 3\frac{\sigma}{S}$$

where σ represents the standard deviation of ten independent measurements of the CD solution in the absence of target ions (n = 10), and S is the slope of the linear calibration curve obtained from the plot of $F_0/F$ versus ion concentration.

To evaluate the $NO_2^-$ sensing performance of the PVA/Alg/CDs film, a 1 × 1 cm piece of the film was immersed in aqueous solutions containing $NO_2^-$ at concentrations ranging from 0 to 50 ppm. After 1 min of exposure, the film was removed and placed in a Petri dish. The film's fluorescence was excited by a 365 nm UV lamp, and digital images were captured with a smartphone. The obtained images were subsequently analyzed using ImageJ software for quantitative colorimetric evaluation.

## 2.6. Selective detection of pollutant ions

For the selectivity evaluation, 1 mL of the as-prepared CD solution (5 $mgL^{-1}$) was mixed with 2 mL of each interfering ion solution, each at 50 ppm. The tested species included $Cu^{2+}$, $Fe^{3+}$, $Fe^{2+}$, $Na^+$, $K^+$, $Ca^{2+}$, $Pb^{2+}$, $NO_2^-$, $NO_3^-$, $Cl^-$, $SO_4^{2-}$, and $CO_3^{2-}$. After incubation at room temperature for 10 min, the photoluminescence spectra of the resulting mixtures were recorded at an excitation wavelength of 320 nm.

# 3. Results and discussion

Figure 1a shows that the synthesized CDs exhibit a uniform and well-dispersed dot-like morphology, with particle sizes ranging from 4 to 8 nm and an average diameter of 6.02 nm. The HR-TEM image (Fig. 1b) reveals clear lattice fringes with an interplanar spacing of approximately 0.21 nm, indicating the crystalline nature of the CDs. This crystalline structure is further confirmed by the corresponding SAED pattern (Fig. 1c), which displays distinct diffraction features characteristic of nanocrystalline carbon. Under UV excitation, the CDs exhibit bright blue fluorescence (Fig. 1d), demonstrating their strong photoluminescence. These results collectively confirm the successful synthesis of uniform, crystalline, and highly emissive CDs.

Figure 2a shows the FTIR spectrum of the CDs, revealing the presence of abundant surface functional groups. The broad absorption band centered at approximately 3300 $cm^{-1}$ is attributed to the stretching vibration of O-H groups. The prominent peak at around 1600 $cm^{-1}$ corresponds to C = O and C = C

stretching vibrations, while the bands at 1342 and 1180 $cm^{-1}$ are assigned to C-N and C-O bonds, respectively. The rich surface chemistry endows the CDs with inherent hydrophilicity and facilitates their uniform dispersion and stable immobilization within the copolymer matrix.

The multiple surface functional groups introduce diverse electronic states, which are reflected in the UV-vis absorption spectrum (Fig. 2b). The CDs exhibit strong absorption in the ultraviolet region with three characteristic peaks. The absorption bands at approximately 300 and 340 nm are ascribed to n→π* transitions associated with nitrogen- and oxygen-containing functional groups, consistent with the FTIR results. In addition, a sharp absorption peak at around 270 nm originates from π→π* transitions of π-conjugated domains in the carbon core. In contrast, the CDs show negligible absorption in the visible region, confirming that their optical response is dominated by ultraviolet excitation.

The PL properties of the CDs are presented in Fig. 2c, revealing two distinct emission regions in the blue and green spectral ranges, indicative of a dual-emission behavior. Under excitation wavelengths from 260 to 380 nm, the CDs exhibit strong blue emission, with the emission peak shifting from approximately 400 to 430 nm, demonstrating a clear excitation-dependent emission characteristic. The maximum blue emission intensity is observed at around 425 nm under 340 nm excitation. In addition to the dominant blue emission, a second emission band in the green region is also detected, although its intensity is significantly weaker under short-wavelength excitation. In contrast, when excited at wavelengths longer than 380 nm, the green emission becomes dominant, exhibiting a strong and well-defined peak centered at approximately 520 nm. Notably, this green emission peak remains excitation-independent, suggesting a different emission origin compared to the blue band.

The distinct excitation behaviors of the two emission peaks can be attributed to their different photoluminescence origins [9]. The excitation-dependent blue emission is associated with core-related electronic states of the CDs, which typically involve multiple discrete energy levels arising from size distribution and quantum confinement effects. Conversely, the excitation-independent green emission is ascribed to surface defect states and functional groups, which form continuous energy levels. Upon excitation, charge carriers relax non-radiatively to the lowest surface energy state prior to photon emission, resulting in a single, fixed emission peak at 520 nm.

Using quinine sulfate as a fluorescence reference, the CDs exhibit a relatively high quantum yield of 24.25%, confirming their strong emissive efficiency and suitability for fluorescence-based sensing applications.

Figures 3a and 3b illustrate the effect of $Fe^{3+}$ ions on the PL spectra of the CDs. A pronounced difference in quenching behavior is observed between the two emission bands. Under 300 nm excitation, the emission peak at 420 nm gradually decreases as the $Fe^{3+}$ concentration increases from 0 to 50 ppm. In contrast, the emission band centered at 520 nm under 460 nm excitation exhibits a much stronger quenching response. Notably, the 520 nm emission is almost completely quenched at $Fe^{3+}$

concentrations as low as 10 ppm and remains suppressed up to 50 ppm, indicating a high sensitivity of this emission channel toward $Fe^{3+}$ ions.

In comparison, the PL response of the CDs toward $NO_2^-$ ions shows a distinctly different behavior. As shown in Figs. 3c and 3d, both emission peaks at 420 nm and 520 nm exhibit a gradual and nearly linear quenching as the $NO_2^-$ concentration increases from 10 to 50 ppm, suggesting a uniform interaction mechanism between $NO_2^-$ ions and the CDs.

Figure 3e presents the linear relationship between the fluorescence quenching efficiency ($F/F_0$) and ion concentration derived from the PL spectra of CDs in the presence of $Fe^{3+}$ and $NO_2^-$. The LODs for $NO_2^-$ and $Fe^{3+}$ were determined to be 0.12 ppm and 0.17 ppm, respectively. Furthermore, the CDs exhibit excellent selectivity toward $NO_2^-$ and $Fe^{3+}$ ions, as demonstrated in Fig. 3f. In the presence of various competing anions and cations at a concentration of 50 ppm, a significant fluorescence quenching is observed only for $NO_2^-$ and $Fe^{3+}$, while other ions induce negligible changes. This high selectivity underscores the strong potential of the CDs as dual-mode fluorescent probes for the selective detection of $NO_2^-$ anions and $Fe^{3+}$ cations in complex aqueous environments.

FT-IR and UV-Vis spectroscopy were employed to elucidate the interaction mechanisms between CDs and the two target ions, $Fe^{3+}$ and $NO_2^-$. As shown in Fig. 4a, the FT-IR spectrum of CDs in the presence of $Fe^{3+}$ does not exhibit the emergence of any new characteristic vibrational bands associated with Fe-ligand covalent bonding [11]. This observation suggests that $Fe^{3+}$ does not induce the formation of new chemical functional groups on the CD surface. However, a pronounced change is observed in the UV-Vis absorption spectrum (Fig. 4b), where the $Fe^{3+}$-CD system displays a significant enhancement in absorbance within the UV region compared to pristine CDs. This absorbance increase can be attributed to the formation of $Fe^{3+}$-CD surface complexes through coordination interactions between $Fe^{3+}$ ions and oxygen- or nitrogen-containing functional groups on the CD surface, such as -COOH, -OH, and $-NH_2$. The complexation process introduces new electronic energy levels and facilitates charge transfer transitions, which have been widely reported in previous studies on $Fe^{3+}$ sensing using carbon-based nanomaterials. As a consequence of these newly formed surface-associated energy states, the surface-state-dominated emission at 520 nm is strongly perturbed, resulting in the complete fluorescence quenching observed in Fig. 3b. This behavior confirms that the green emission band is highly sensitive to surface coordination effects induced by $Fe^{3+}$ ions.

In contrast, the interaction mechanism between CDs and $NO_2^-$ ions is fundamentally different. As shown in Fig. 4a, the FT-IR spectrum of CDs after exposure to $NO_2^-$ reveals the appearance of a new absorption band centered at approximately 2100 $cm^{-1}$. This band can be attributed to the attachment of $NO_2^-$ species onto the hexagonal ring structure of the CD core [25], indicating the formation of $NO_2^-$ related surface species. The emergence of this new band provides direct evidence for a chemical modification of the CD surface induced by $NO_2^-$.

Consistent with the FT-IR results, the UV-Vis spectrum (Fig. 4b) shows the appearance of a strong absorption peak around 380 nm following $NO_2^-$ addition. This new absorption feature is attributed to electronic transitions associated with the newly formed $NO_2^-$ surface groups. The formation of these species is likely driven by the nitrosation or oxidation of surface -$NH_2$ groups on the CDs by $NO_2^-$ ions, leading to the conversion of amino functionalities into nitrogen-oxygen-containing moieties. This chemical transformation alters the surface electronic structure of the CDs, thereby affecting both the blue (420 nm) and green (520 nm) emission channels and leading to the simultaneous, linear quenching behavior observed in Figs. 3c and 3d.

Figure 5 presents a comprehensive physicochemical and optical characterization of the PVA/Alg/CDs composite film. The water contact angle of the film was measured to be 52° (Fig. 5a), indicating a moderately hydrophilic surface character attributable to the abundant hydroxyl (-OH) and carboxylate (-COOH) functional groups inherent to the PVA/alginate polymer network. This hydrophilicity facilitates favorable interfacial interactions with aqueous media and promotes rapid diffusion of target ions into the sensing layer. Mechanical characterization via tensile testing (Fig. 5b) yielded a tensile strength of 5.76 MPa and an elongation at break of 192.1%, demonstrating that the film possesses both adequate structural integrity and pronounced flexibility. These mechanical properties are attributed to the interpenetrating polymer network formed between the ionically $Ca^{2+}$-crosslinked alginate chains, which confer structural rigidity, and the flexible PVA segments, which contribute to overall elasticity, rendering the composite film suitable for practical solid-state sensing applications. The swelling degree was determined to be 66.7% ($W_{dry}$ = 0.2543 g; $W_{swollen}$ = 0.4238 g), reflecting a moderate yet significant water uptake capacity that generates internal diffusion channels facilitating the rapid penetration and interaction of analyte ions with the embedded CDs. Digital photographs of the dry and swollen films under visible light (Fig. 5c) reveal a homogeneous pale yellow appearance in both states, confirming uniform film formation and structural stability upon hydration. Under 365 nm UV excitation (Fig. 5d), both the dry and swollen films exhibit strong and uniform blue fluorescence, providing direct visual evidence of effective CD immobilization within the polymer matrix without observable aggregation or leaching. The preservation of intense fluorescence emission in the swollen state further confirms the structural robustness of the crosslinked PVA/alginate network as a stable host for CD confinement, highlighting its strong potential as a portable, low-background solid-state platform for on-site water quality monitoring.

To enable practical applications, the CDs were embedded into a PVA/alginate copolymer matrix to fabricate a flexible PVA/Alg/CDs composite film. Under visible light illumination, the PVA/Alg/CDs composite film presents a homogeneous pale yellow appearance, while strong and uniform blue fluorescence emission is observed across the entire film surface upon excitation with a 365 nm UV lamp, as shown in Fig. 6a. Upon exposure to increasing concentrations of $NO_2^-$ ions, the fluorescence intensity of the film undergoes a progressive and concentration-dependent quenching, providing a clear visual signal readily discernible to the naked eye. The film exhibited an immediate fluorescence quenching response upon contact with $NO_2^-$ ions, as demonstrated in Fig. 6b and Supporting Video S1, confirming that $NO_2^-$ ions diffuse rapidly through the hydrated PVA/alginate polymer network and interact efficiently

with the surface-active sites of the immobilized CDs. For comparison, direct exposure of the CD solution to $Fe^{3+}$ ions resulted in an instantaneous and near-complete fluorescence quenching (Supporting Video S2), confirming the exceptional sensitivity of the CDs toward $Fe^{3+}$ in the solution phase via surface coordination-induced charge transfer. In stark contrast, the PVA/Alg/CDs composite film displayed no discernible change in fluorescence emission upon prolonged exposure to $Fe^{3+}$ ions under identical experimental conditions, demonstrating that the crosslinked polymer matrix effectively prevents $Fe^{3+}$ from accessing the encapsulated CDs. This selective ion-exclusion behavior is ascribed to the densely crosslinked ionic network established through $Ca^{2+}$-mediated coordination of alginate carboxylate groups. Given the higher charge density and stronger Lewis acid character of $Fe^{3+}$ relative to $Ca^{2+}$, incoming $Fe^{3+}$ ions are preferentially sequestered at the outer surface of the film through competitive complexation with the carboxylate-rich alginate chains, effectively precluding their penetration into the bulk polymer matrix where the CDs are embedded. This intrinsic ion-gating mechanism thus confers remarkable analyte selectivity upon the composite film, enabling an exclusive fluorescence response toward $NO_2^-$ while maintaining complete insensitivity to $Fe^{3+}$, a property of considerable practical significance for the development of selective solid-state sensors for on-site water quality monitoring.

PL spectra in Fig. 6c reveal a slight red shift of the emission peak from 420 nm for pristine CDs to approximately 430 nm after incorporation into the PVA/Alginate matrix. This shift may be attributed to changes in the local microenvironment and polymer-induced surface interactions. Importantly, the fluorescence-quenching behavior toward $NO_2^-$ remains preserved after film formation.

To quantitatively evaluate the color change, both spectroscopic analysis and smartphone-assisted image analysis were employed. As shown in Fig. 6d, the overall fluorescence intensity extracted using ChatGPT-assisted RGB analysis and ImageJ processing shows a consistent decreasing trend with increasing $NO_2^-$ concentration, in good agreement with the spectroscopic results. Figure 6e presents the linear relationship between fluorescence quenching efficiency $F/F_0$ and ion concentration. All three analytical approaches exhibit excellent linearity over the concentration range from 0 to 50 ppm, with coefficients of determination exceeding 0.93. These findings demonstrate that the PVA/Alg/CDs film is highly promising for smartphone-based, on-site detection of $NO_2^-$ in aqueous environments.

# 4. Conclusions

In this study, dual-emission CDs were successfully synthesized and applied for the selective detection and discrimination of $Fe^{3+}$ and $NO_2^-$ ions. The CDs exhibited two distinct emission bands at approximately 420 nm and 520 nm, enabling differentiated quenching responses toward the two analytes. The fluorescence quenching efficiency showed excellent linear correlations with ion concentration, achieving low detection limits of 0.12 ppm for $NO_2^-$ and 0.17 ppm for $Fe^{3+}$. Besides, the PVA/Alg/CDs composite film displayed strong blue emission under 365 nm UV excitation and demonstrated rapid fluorescence quenching upon exposure to $NO_2^-$. The film exhibited clear concentration-dependent intensity changes, with overall fluorescence intensity decreasing as $NO_2^-$

concentration increased from 0 to 50 ppm, showing excellent linearity with $R^2 > 0.93$. Importantly, smartphone-assisted RGB image analysis produced quantitative results consistent with spectroscopic measurements, confirming the feasibility of portable detection. These results demonstrate that the PVA/Alg/CDs film offers a stable, low-background, and solid platform for on-site monitoring of hazardous ions in water.

## Declarations

# Author Contribution

Nguyen Ba Hung: Conceptualization, Investigation, supervision, project administration, writing review and editing.Duong Duy Son: Investigation, methodology, formal analysis.Vu Tan Phat: Software development, data analysis.Do Anh Viet: Validation, formal analysis.Tran Thi Bich Lan: Resources, investigation.Luu Thi Van: Data curation, visualization.Ban Dieu Linh: Data curation, visualization.Nguyen Tri Nghia: Resources, supervision.Nguyen Minh Hoang: Conceptualization, methodology, investigation, data curation, writing original draft, writing review, and editing.

# Acknowledgments

We acknowledge the support from Vietnam Military Medical University under Decision No. 1058/QĐ-HVQY for the project entitled “Chế tạo màng Polyvinyl alcohol/Alginate@CDs ứng dụng trong phát hiện ion nitrit ($NO_2^-$) trong nước”.

## References

1. A. Chamoli, A. Bhambri, S.K. Karn, V. Raj, Ammonia, nitrite transformations and their fixation by different biological and chemical agents, *Chemistry and Ecology* 40 (2024) 166-199.
2. P. Sahu, A.R. Patel, A. Pandey, M. Hait, G.K. Patra, Assessment of heavy metal ion toxicity in wastewater: A comprehensive review, *Inorganica Chimica Acta* 585 (2025).
3. A.M. Fan, Nitrate and Nitrite in Drinking Water: A Toxicological Review, Encyclopedia of Environmental Health, Volume 1-52011, pp. V4-137.
4. C.J. Kotalik, P. Cadmus, W.H. Clements, Indirect Effects of Iron Oxide on Stream Benthic Communities: Capturing Ecological Complexity with Controlled Mesocosm Experiments, *Environmental Science and Technology* 53 (2019) 11532-11540.
5. Y. Kanda, M. Taira, Flow-injection analysis method for the determination of nitrite and nitrate in natural water samples using a chemiluminescence NOx monitor, *Analytical Sciences* 19 (2003) 695-699.
6. M. Shahbaz, U. Salma, M.Z. Alam, M.A. Mujeeb, R.u.H. Ansari, H.A. Basha, Alimuddin, S.A. Khan, Fluorescent/Photoluminescent Carbon Dots as a Sensor for the Selective and Sensitive Detection of

Fe3+/Fe2+ Metal Ions. A Review of the Last Decade, *Journal of Fluorescence* (2025) 1-24.

7. M.K. Goshisht, N. Tripathi, Fluorescence-based sensors as an emerging tool for anion detection: mechanism, sensory materials and applications, *Journal of Materials Chemistry C* 9 (2021) 9820-9850.
8. N. Ullah, M. Mansha, I. Khan, A. Qurashi, Nanomaterial-based optical chemical sensors for the detection of heavy metals in water: Recent advances and challenges, *TrAC Trends in Analytical Chemistry* 100 (2018) 155-166.
9. N.M. Hoang, N.T.B. Ngoc, N.-A. Tran, N.X. Ho, H.-L.T. Dang, D.V. Cuong, V.T. Trang, P.T.L. Huong, P.T.T. Huyen, M.S.J.J.o.E.C.E. Jamil, Dual-Emission Carbon Dots: Synthesis, Applications, Advances and Challenges, (2025) 117696.
10. L. Wang, J. Jana, J.S. Chung, W.M. Choi, S.H. Hur, Designing an intriguingly fluorescent N, B-doped carbon dots based fluorescent probe for selective detection of NO2− ions, *Spectrochimica Acta Part A: Molecular and Biomolecular Spectroscopy* 268 (2022) 120657.
11. N.T.B. Ngoc, V.T.H. Ha, T.N. Anh, N.M. Hoang, V.-D.J.M.J. Dao, Rare emission peak shift unlocks detection of multiple heavy metal ions with dual emission carbon dots, (2025) 115776.
12. Y. Liu, S. Luo, P. Wu, C. Ma, X. Wu, M. Xu, W. Li, S. Liu, Hydrothermal synthesis of green fluorescent nitrogen doped carbon dots for the detection of nitrite and multicolor cellular imaging, *Analytica chimica acta* 1090 (2019) 133-142.
13. B.-B. Chen, M.-L. Liu, Y.-T. Gao, S. Chang, R.-C. Qian, D.-W. Li, Design and applications of carbon dots-based ratiometric fluorescent probes: A review, *Nano Research* 16 (2023) 1064-1083.
14. Z.-f. Cheng, X.-y. Wu, L. Liu, L. He, Z.-g. Yang, C. Cao, Y. Lu, J.-x. Guo, A highly efficient, rapid, room temperature synthesis method for coal-based water-soluble fluorescent carbon dots and its use in Fe3+ ion detection, *New Carbon Materials* 38 (2023) 1104-1115.
15. L. Xu, Z. Zheng, L. Fang, J. Zhou, X. Zheng, Q. Gao, C. Xu, Characterization of cellulose-derived carbon dots/polyvinyl alcohol films and their application in blueberry preservation, *International Journal of Biological Macromolecules* (2025) 144798.
16. H. Bai, X. Wu, J. Hou, Y. Chen, D. Zhu, G. Wang, Polyvinyl Alcohol Luminescent Composite Fibers Based on Room Temperature Phosphorescent Carbon Dots, *Colloids Surfaces A: Physicochemical Engineering Aspects* (2025) 138098.
17. Z. Chen, Y. Zhang, X. Feng, X. Cui, H. Xiao, A. Yang, M. Xie, R. Xiong, W. Cheng, C. Huang, Biomass based nanofiber membrane composite with xylan derived carbon dots for fluorescence detection nitrite in food real samples, *International Journal of Biological Macromolecules* 280 (2024) 135693.
18. S. Liu, G. Du, X. Ran, H. Yang, J. Yuan, Y. Wu, J. Li, X. Lin, W. Gao, L. Yang, Visual, customizable wood-based colorimetric test paper encapsulated with fluorescent carbon dots for rapid explosive detection, *Industrial Crops and Products* 194 (2023) 116398.
19. Y.J. Fan, Z.G. Wang, M. Su, X.T. Liu, S.G. Shen, J.X. Dong, A dual-signal fluorescent colorimetric tetracyclines sensor based on multicolor carbon dots as probes and smartphone-assisted visual assay, *Analytica Chimica Acta* 1247 (2023) 340843.

20. H.O. Othman, Fe-doped red fluorescent carbon dots for caffeine analysis in energy drinks using a paper-based sensor, *Journal of Fluorescence* 35 (2025) 7059-7071.
21. L. Zhao, M. Zhang, A.S. Mujumdar, B. Adhikari, H. Wang, Preparation of a novel carbon dot/polyvinyl alcohol composite film and its application in food preservation, *ACS Applied Materials & Interfaces* 14 (2022) 37528-37539.
22. J. Zhang, L. Gu, Y. Zhao, M.H. Nawaz, W. Xia, P. Wang, G. Yang, X. Shen, C. Fan, C. Kong, Fluorescence-Enhanced Carbon Dots/Silica Aerogel-Loaded PVA Sensor for On-site Detection of Biogenic Amines in Aquatic Products, *Food Analytical Methods* 18 (2025) 2470-2486.
23. G. Murugan, A. Khan, K. Nilsuwan, J.T. Kim, S. Benjakul, J.-W. Rhim, Chitosan/polyvinyl alcohol based blend film containing tangerine peel carbon dots: Properties, antioxidant and antibacterial activities, *Waste Biomass Valorization* 16 (2025) 2255-2270.
24. N.M. Hoang, N.T.B. Ngoc, P.T.L. Huong, P.T.T. Huyen, D.Q. Duy, V.-D. Dao, L.T. Tu, Dual Emission Carbon Dots for Simultaneous Detections of Pb2+ and Fe3+ Ions in Water Via Distinct Sensing Mechanisms, *JFlu* (2023).
25. G. Marussi, D. Vione, Secondary Formation of Aromatic Nitroderivatives of Environmental Concern: Photonitration Processes Triggered by the Photolysis of Nitrate and Nitrite Ions in Aqueous Solution, *Molecules* 26 (2021) 2550.

# Figures

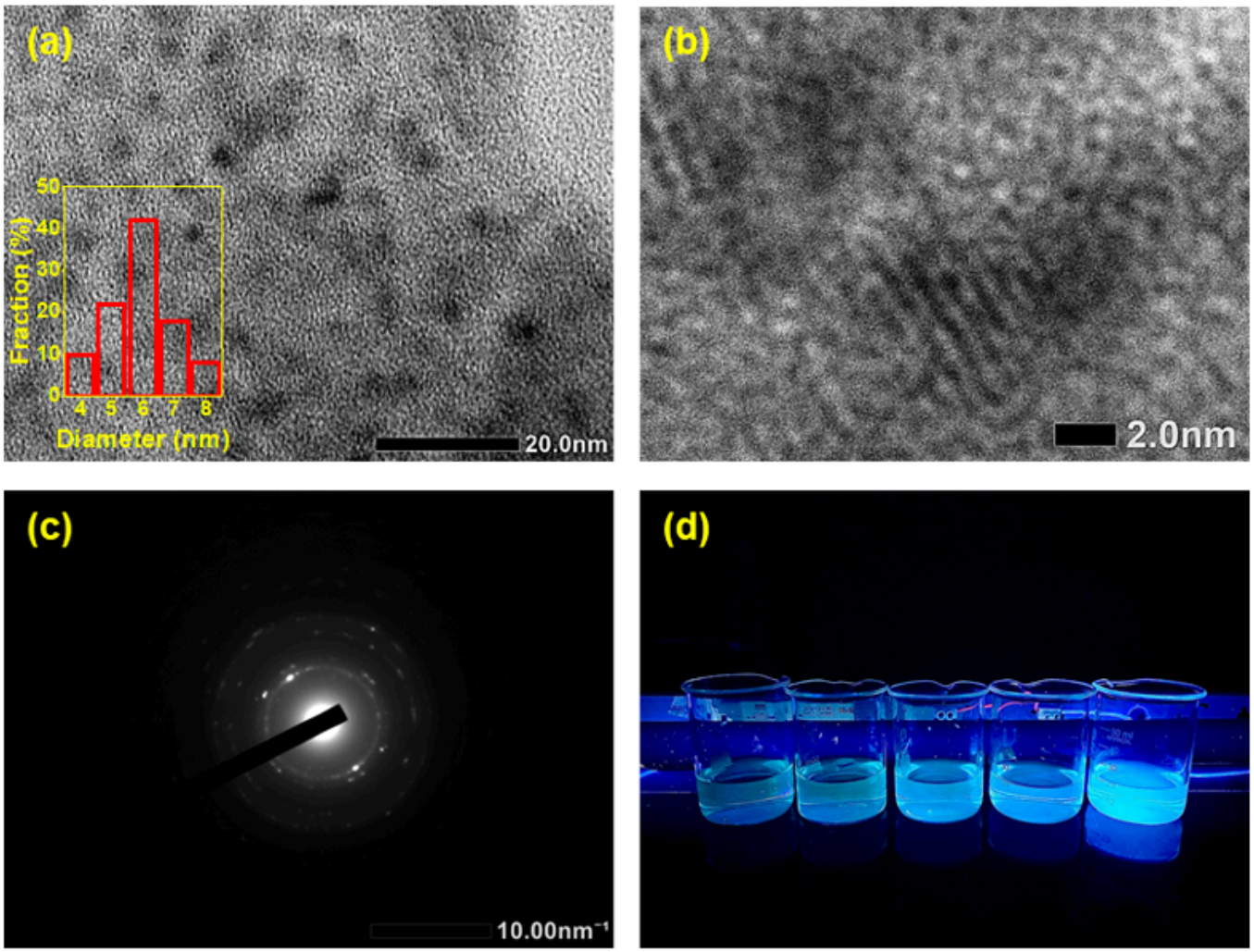
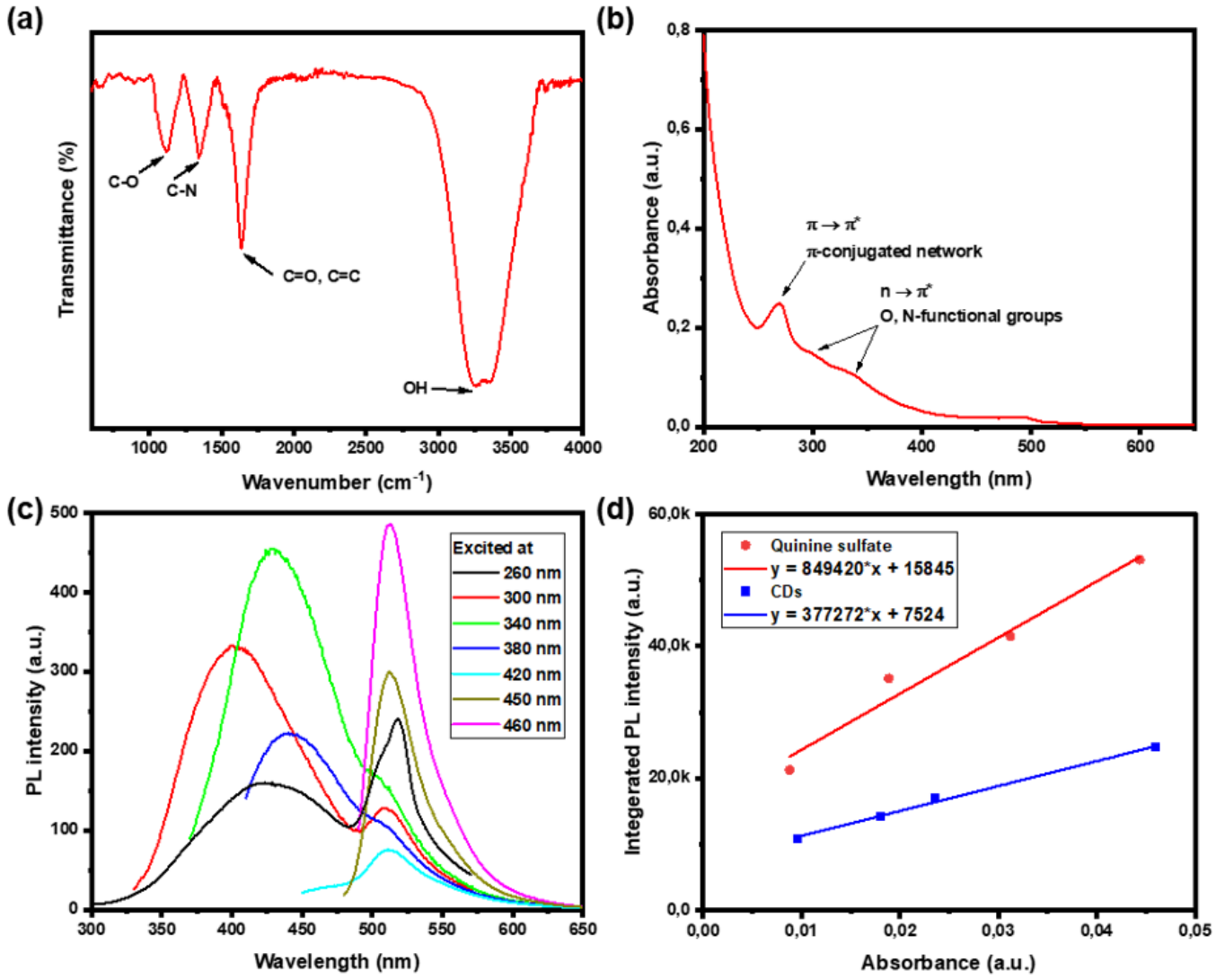


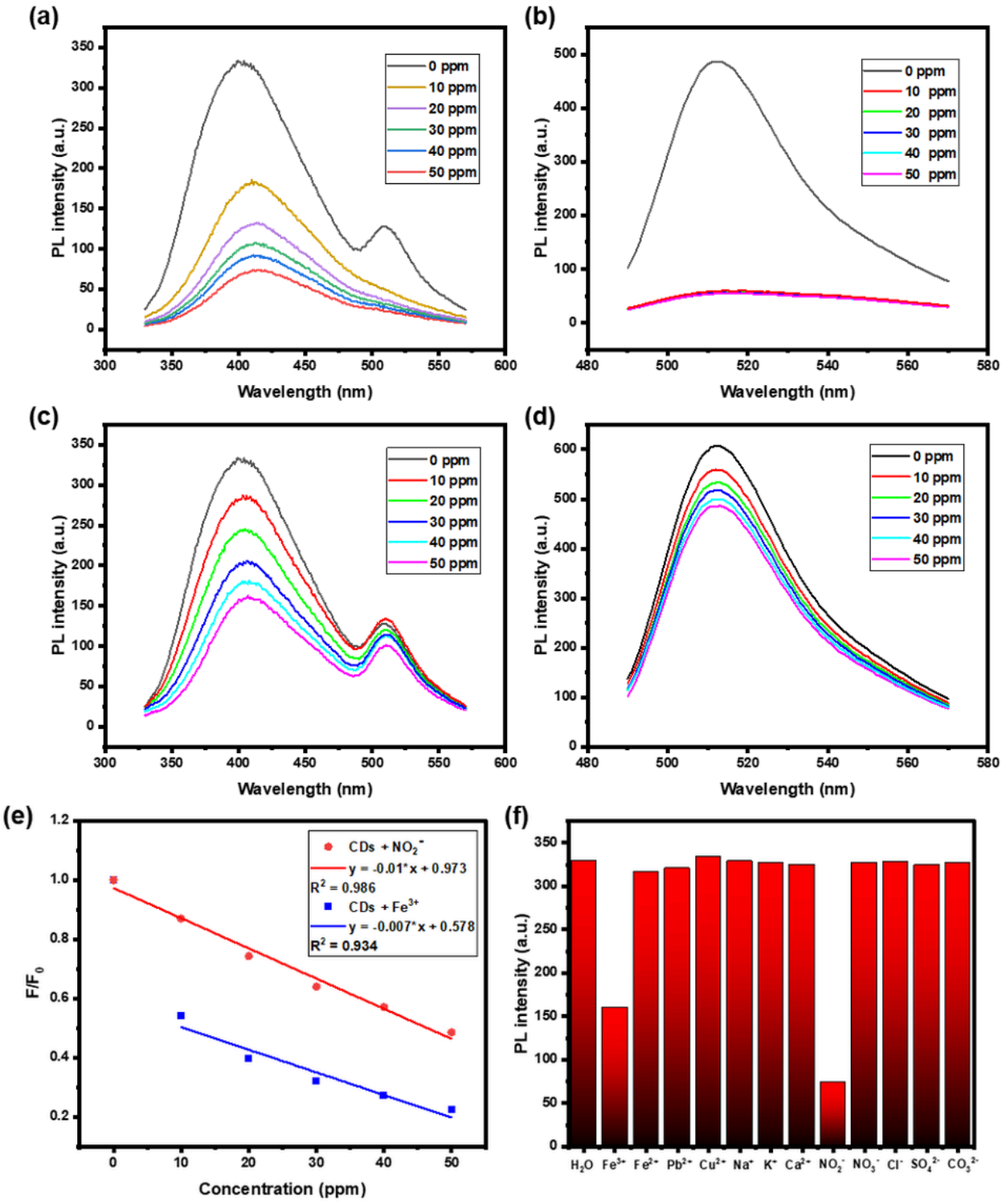

**Figure 1**

(a) HR-TEM image of CDs and the corresponding particle size distribution. (b) HR-TEM image revealing the crystalline lattice structure of CDs. (c) SAED pattern of CDs. (d) Digital image of CDs exhibiting bright blue fluorescence under 365 nm UV light.




## Figure 2

(a) FT-IR spectrum and (b) UV-Vis absorption spectrum of CDs. (c) PL spectra of CDs under different excitation wavelengths. (d) Comparison of the quantum yields of CDs and quinine sulfate.




## Figure 3

PL emission spectra of CDs in the presence of different Fe3+ concentrations under excitation at (a) 300 nm and (b) 460 nm. PL emission spectra of CDs in the presence of different concentrations under excitation at (c) 300 nm and (d) 460 nm. (e) Linear relationship between fluorescence quenching efficiency (F/F0) and ion concentration. (f) Selectivity of CDs toward various metal ions and anions with a concentration of 50 ppm.

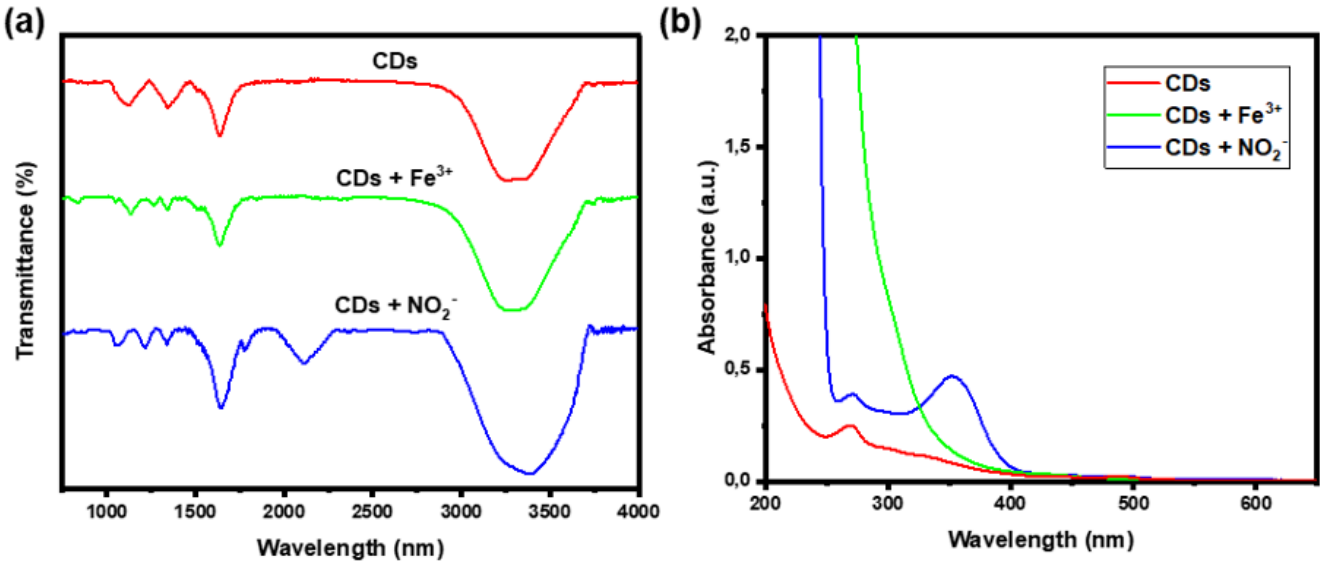



**Figure 4**

(a) FT-IR spectra and (b) UV-Vis absorption spectra of CDs before and after interaction with $Fe^{3+}$ and $NO_2$-ions.

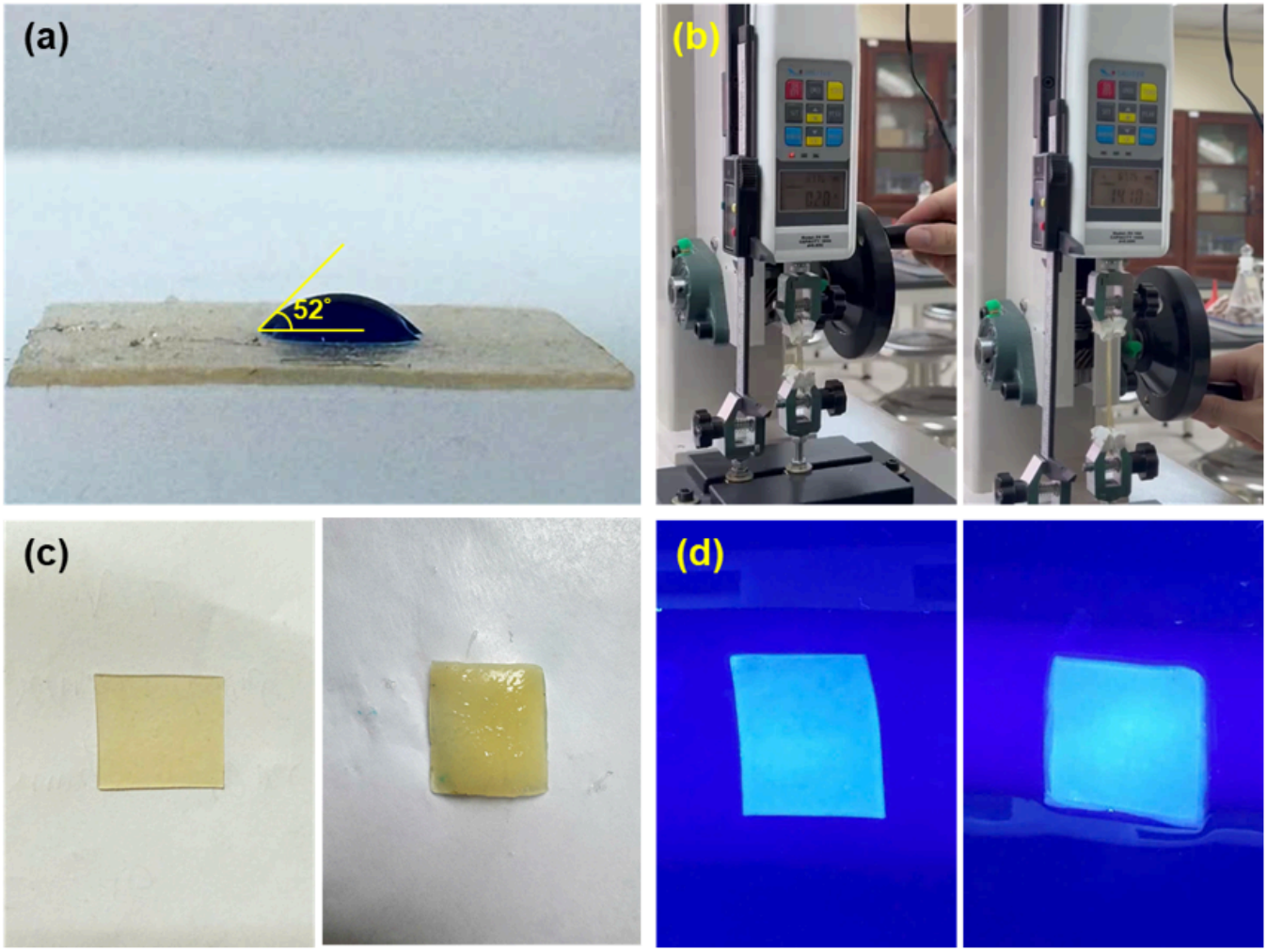



**Figure 5**

(a) The water contact angle of the PVA/Alg/CDs composite film. (b) The stress test of the film. The digital photos of the dry and wet films in the daylight (c) and (d) under UV lamp excitation.

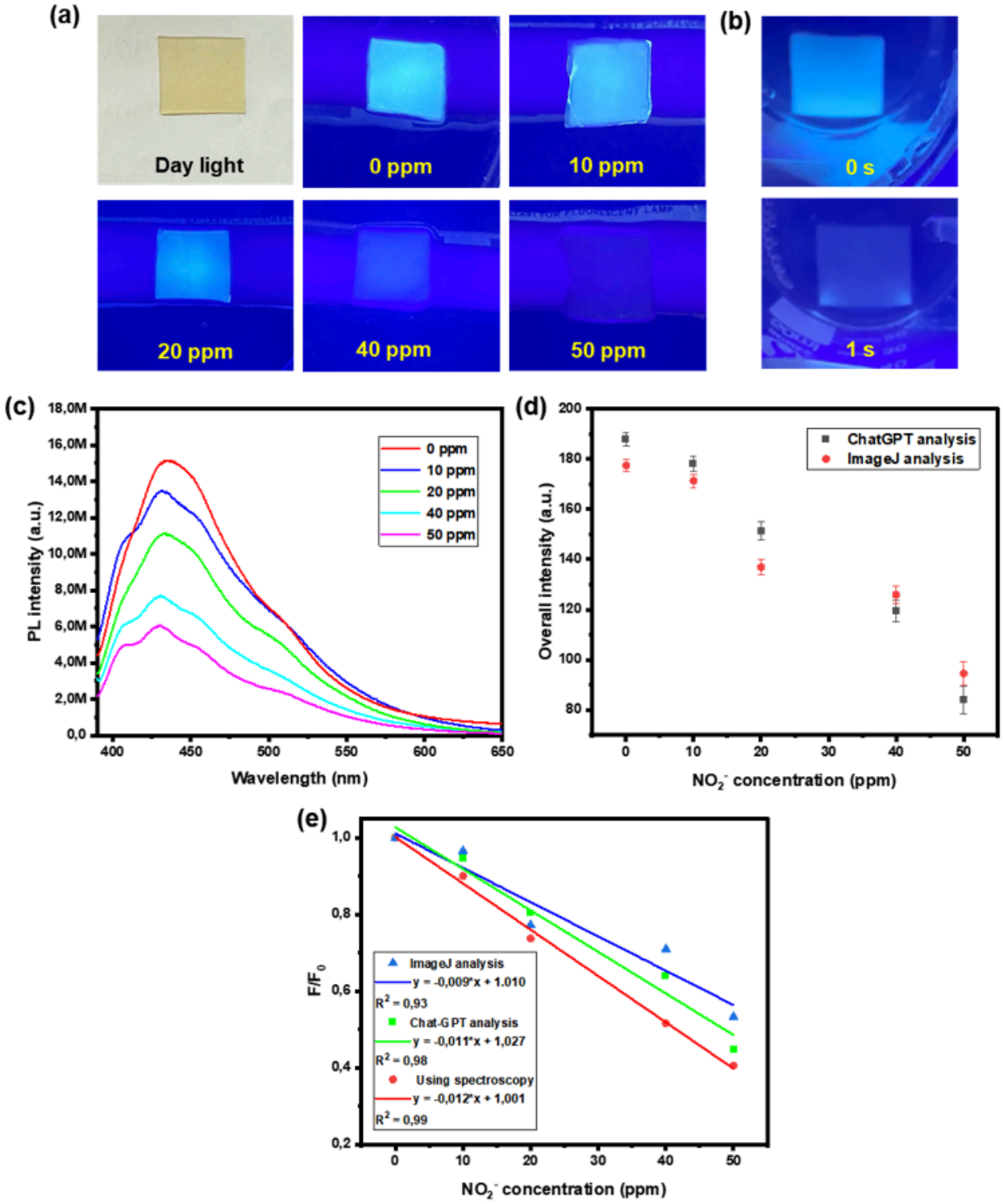



**Figure 6**

(a) Digital photos of the PVA/Alg/CDs composite film under visible light and UV illumination after exposure to different $NO_2$-concentrations. (d) The rapid fluorescence-quenching behavior of the PVA/Alg/CDs film upon contact with $NO_2$-ions. (c) PL spectra of the PVA/Alg/CDs film in response to varying concentrations. (d) PL intensity analysis using Chat-GPT. (e) Linear relationship between fluorescence quenching efficiency (F/F0) and ion concentration.

## Supplementary Files

This is a list of supplementary files associated with this preprint. Click to download.

- VideosupportingS1.mov
- VideosupportingS2.mp4
- Graphicalabstract.docx